This paper is presented here for review only and will be published in the IEEE-MTT Oct.'93 Special Issue on Quasi-Optical Techniques.

Double-Slot Antennas on Extended Hemispherical and Elliptical Silicon Dielectric Lenses

Daniel F. Filipovic, STUDENT MEMBER, IEEE,
Steven S. Gearhart, STUDENT MEMBER, IEEE,
and Gabriel M. Rebeiz, MEMBER, IEEE.

NASA/Center for Space Terahertz Technology
Electrical Engineering and Computer Science Department
University of Michigan
Ann Arbor, MI 48109-2122

ABSTRACT

In this paper, the far-field patterns and Gaussian-beam coupling efficiencies are investigated for a double-slot antenna placed on hemispherical lenses with varying extension lengths. The radiation patterns of a double-slot antenna on a silicon dielectric lens are computed using ray-tracing inside the dielectric lens and electric and magnetic field integration on the spherical dielectric surface. The measured radiation patterns at 246GHz and Gaussian-beam coupling efficiencies show good agreement with theory. The theoretical results are presented in extension length/radius and radius/λ and therefore result in universal design curves for silicon lenses of different diameters and at different frequencies. The theoretical and experimental results indicate that for *single units*, there exists a wide range of extension lengths (ext. length/radius=0.32 to 0.35) which result in high Gaussian-coupling efficiencies (50-60%) to moderately high f#'s. These Gaussian-coupling efficiencies can be increased to 80-90% with the use of a $\lambda_m/4$ matching-cap layer. For *imaging array* applications with high packing densities, an extension length/radius=0.38 to 0.39 (depending on frequency) will result in peak directivity and a corresponding Gaussian-coupling efficiency 15-20% lower than for single units.

I. INTRODUCTION

Integrated antennas on thick dielectric substrates suffer from power loss into substrate modes [1,2]. One way to avoid this problem is to integrate the antennas on a very thin substrate, typically less than $.02\lambda_d$ for dipoles and $.04\lambda_d$ for slot antennas. However, the substrates become very thin and fragile at millimeter and submillimeter-wavelengths. One way to synthesize a thin substrate is to place the antenna on a very thin dielectric membrane [3,4,5], which is typically between 1-3μm thick. The membranes are integrated on silicon or GaAs wafers and the antennas radiate as if suspended in free-space. Therefore appropriate design methods must be used to render the patterns unidirectional. Another attractive method to eliminate substrate modes is to place the antenna on a dielectric lens. The dielectric lens has the same dielectric constant as the planar antenna wafer. The structure of the dielectric lens does not support surface-waves. Antennas placed on dielectric lenses tend to radiate most of their power into the dielectric side making the pattern unidirectional on high dielectric constant lenses. The ratio of powers between the dielectric and air is $\epsilon_r^{3/2}$ for an elementary slot antenna and ϵ_r for an elementary dipole antenna [1], where ϵ_r is the relative dielectric constant of the lens. The dielectric lens is a very attractive solution since it also provides mechanical rigidity and thermal stability.

Dielectric lenses can be hemispherical, hyperhemispherical, or ellipsoidal, and many researchers have placed various antennas on these lenses for receiver applications. The hyperhemispherical lens is a hemispherical lens with an attached extension length of R/n, where n is the index of refraction of the lens, and R is the radius of the lens. The hyperhemispherical lens was borrowed into the millimeter-wave field from optics [1,6] and it was found that radiation patterns from these lenses were broad and even multi-lobed in some cases. The hyperhemispherical lens satisfies the *sine condition*, which guarantees the absence of circular coma, and is aplanatic, implying the absence of spherical abberations [7]. The latter condition implies that if an optical system is designed such that all the rays are being focused to a point, the hyperhemispherical lens can be added to the system and all the rays will still focus to a point. In antenna terms, the hyperhemispherically shaped dielectric lens bends the rays radiated by the integrated antenna towards the broadside direction, thereby sharpening the pattern and effectively increasing the gain of the integrated antenna by n^2. The hyperhemispherical lens is capable of coupling well to a Gaussian-beam system, but couples well to a converging beam and not to a planar equiphase front. On the other hand, any antenna placed at the focus of the elliptical lens will result in a far-field pattern with a main-beam that is diffraction limited by the aperture of the elliptical lens. In a ray analysis, an elliptical lens with a source at its more distant focus refracts the emitted rays so that they emerge from the lens parallel to each other [8]. The diffraction-limited patterns have been verified for the log-periodic and spiral antennas [9], and also for a simple dipole antenna [10], a double-dipole antenna [11], and a double-slot antenna [12]. The difference between these antennas is in the sidelobe and cross-polarization levels. The elliptical lens is compatible with a large f-number imaging system due to the potential of achieving very narrow beam patterns. As will be seen later, the elliptical lens couples well to a Gaussian-beam at its minimum waist (where there is a planar equiphase front).

The log-periodic [13], spiral [14], double-slot, and double-dipole antennas have been successfully used on quartz and silicon dielectric lenses from 30GHz to 600GHz [15,16,17,18]. The antennas were placed on hyperhemispherical or elliptical dielectric lenses and were characterized by the measured far-field pattern. Recently, Büttgenbach experimentally placed a spiral antenna at a specific position behind the hyperhemispherical point (but before the elliptical focus) and achieved good patterns and a high-aperture efficiency (coupling to a plane wave)[19]. Büttgenbach based his analysis on the quality of the measured far-field power patterns and therefore did not present a full characterization of the Gaussian-coupling efficiency of an extended hemispherical lens.

The need for a full characterization of the extended hemisphere (Fig. 1) prompted us to develop a ray-optics/field-integration formulation to solve for the radiation patterns and Gaussian-coupling efficiencies of a double-slot antenna on hemispherical lenses with a varying extension length. The extended hemispherical system is very practical, since it results in an antenna/lens system which couples to a wide range of quasi-optical systems simply by varying the extension length behind the hemispherical position. It is important to note that the hyperhemispherical lens is a special case of the extended hemispherical lens. Section II shows that there also exists a specific extension length that effectively synthesizes an elliptical lens. Section III presents the theoretical analysis of extended hemispherical lenses and shows the directivity and maximum "Gaussicity" as a function of the extension length. The term "Gaussicity" is defined as the coupling efficiency of a far-field pattern of an antenna to the far-field pattern of a Gaussian-beam. The Gaussian-coupling efficiency is defined as the total coupling efficiency which is the Gaussicity multiplied by any system losses (reflection loss, backside loss, impedance mismatch loss, etc.). Section IV shows the reflection loss with and without a matching-cap layer. Section V describes the directivities and Gaussicities versus extension length as a funcion of frequency. Three particular values of extension length, 1700μm, 2200μm, and 2700μm were chosen for experimental verification. Section VI describes the measured radiation patterns at 246GHz and compares them with theory. Section VII presents the experimental setup at 246GHz used for measuring the Gaussian-coupling efficiency of an extended hemispherical lens. The theoretical and experimental results indicate that with a well designed quasi-optical system, there exists a wide range of extension lengths which yield a high Gaussian-coupling efficiency.

II. SYNTHESIS OF AN ELLIPTICAL LENS

In this section, an elliptical lens is synthesized from an extended hemispherical lens by carefully choosing a particular extension length. The analysis is done in two dimensions since the geometry is rotationally symmetric. The defining equation for an ellipse is:

$$(\frac{x}{a})^2 + (\frac{y}{b})^2 = 1 \tag{1}$$

where the foci are at $\pm c$ and $c = \sqrt{b^2 - a^2}$. It is also known from optics that for a given index of refraction n, the eccentricity of the ellipse such that the geometric focus becomes

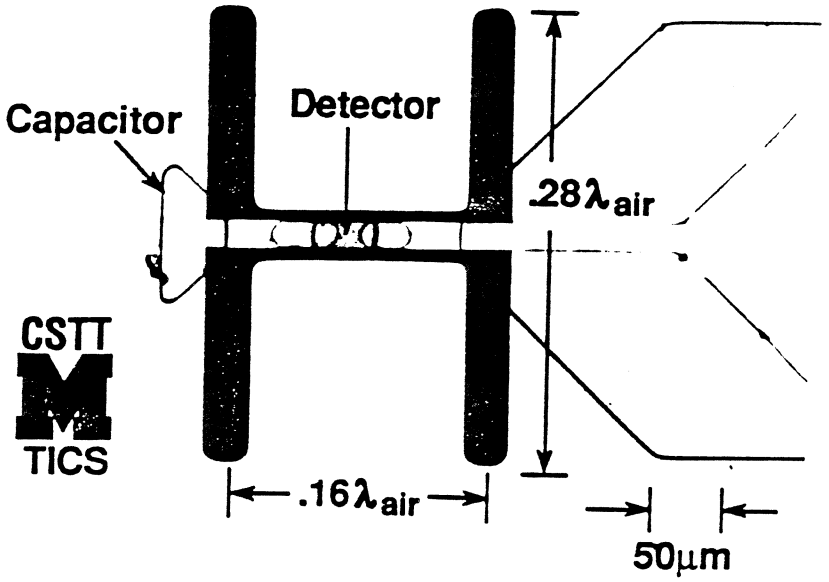

(a)

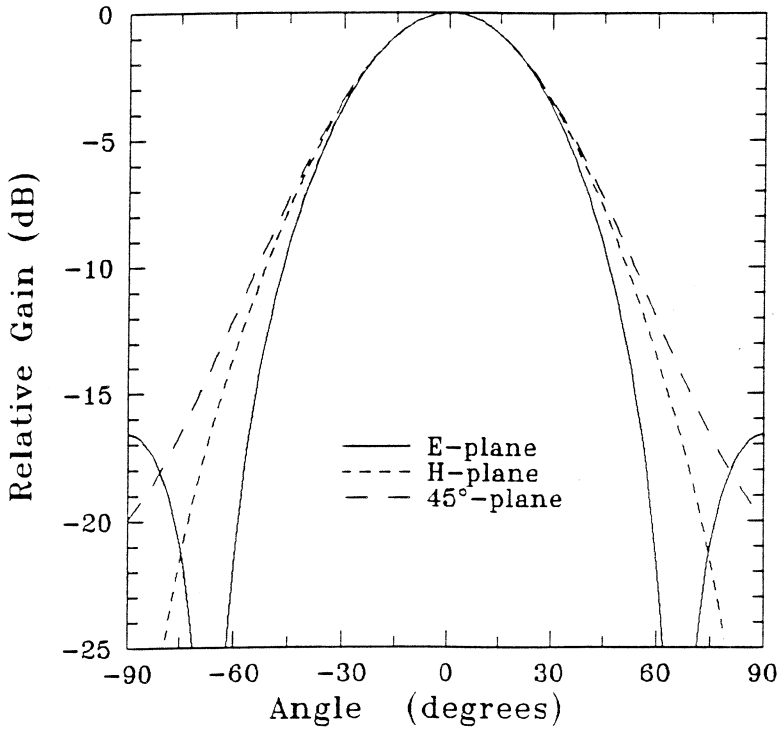

(b)

Figure 3: The double-slot antenna (a) and its radiation patterns into a silicon (ϵ_r=11.7) dielectric (b).

the optical focus is [8] :

$$\text{eccentricity} = \frac{\sqrt{b^2 - a^2}}{b} = \frac{1}{n} \tag{2}$$

From this one can derive that:

$$b = \frac{a}{\sqrt{1 - \frac{1}{n^2}}} \tag{3}$$

$$c = \frac{b}{n} \tag{4}$$

A hemisphere of unit radius is defined by $x^2 + y^2 = 1$, choosing only positive y-values. The distance from the circular tip of an extended hemisphere to the end of its extension is equal to $1 + L$, where L is the extension length. The distance from the tip of an ellipse to its more distant focus is equal to $b + c$. These distances must be equal in order to superimpose the two lenses, which yields $L = 1 - b - c$. The ellipse must be shifted down by a value $y_0 = L - c$ so that the focus of the ellipse has the same coordinates as the focus of the extended hemisphere. Thus given the index of refraction, the parameter b is varied until the extended hemisphere appears to have the closest geometrical match to an ellipse (b will lie within a narrow range no matter how this is defined). This has been done for a dielectric constant of ϵ_r =2.3 (polyethylene), 4.0 (quartz), and 11.7 (silicon), and is shown in Fig. 2. It is obvious that the higher dielectric constant yields a more exact geometrical approximation. For a silicon lens, the fitted ellipse values are a=1.03 and b=1.07691, and this yields an extension length of $L = 2670\mu m$ for a 13.7mm diameter lens. There are many ways to synthesize an ellipse [19] and it will be shown later that the synthesized silicon ellipse presented above is a very good appoximation to a true elliptical lens.

III. THEORETICAL ANALYSIS

A double-slot antenna is chosen as the feed antenna for the extended hemispherical lenses. This antenna has been used previously by Kerr et. al. in a 100GHz receiver [20] and recently Zmudzinas built a 492 GHz SIS receiver using a double-slot antenna on a quartz hyperhemispherical lens [17]. The double-slot antenna patterns are calculated assuming a sinusoidal magnetic current distribution on the slot and using an array factor in the E-plane direction [21]. The double slots lie in the x-z plane, and the slots point in the direction of the z-axis. The wavelength of the sinusoidal current distribution in the slot is the mean wavelength [22] given by $\lambda_m = \lambda_0/\sqrt{\epsilon_m}$ and $\epsilon_m = (1 + \epsilon_r)/2$. The current in the slot is given by :

$$I = I_{max}\sin[k_m(l - |z|)], \qquad l \le z \le l, \qquad l_{max} = 0.28\lambda_{air} \tag{5}$$

where $k_m = 2\pi/\lambda_m$. The corresponding normalized H-plane field pattern is:

$$\frac{\sin\theta[\cos(k_e l\cos\theta) - \cos(k_m l)]}{k_m^2 - k_e^2\cos^2\theta} \tag{6}$$

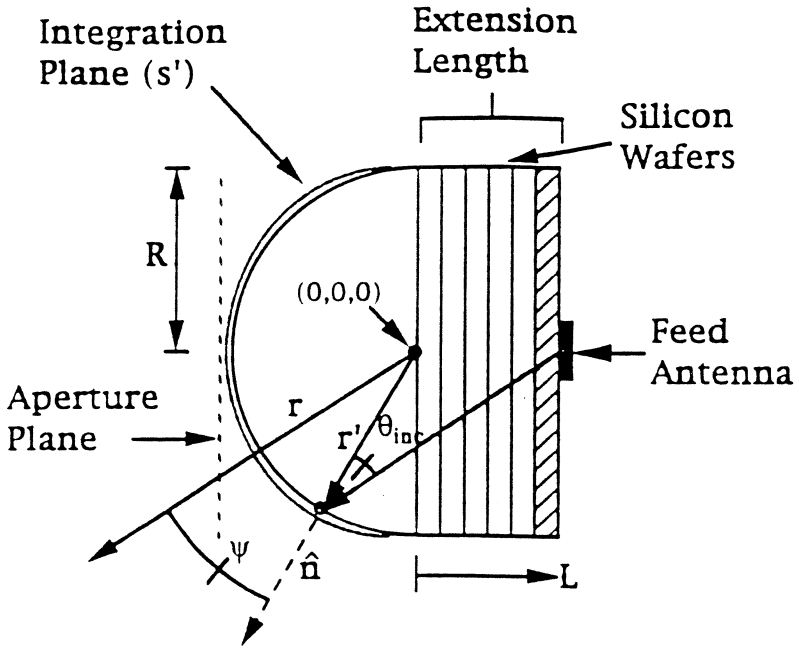

Figure 1: The extended hemispherical lens and the ray-tracing/field-integration technique.

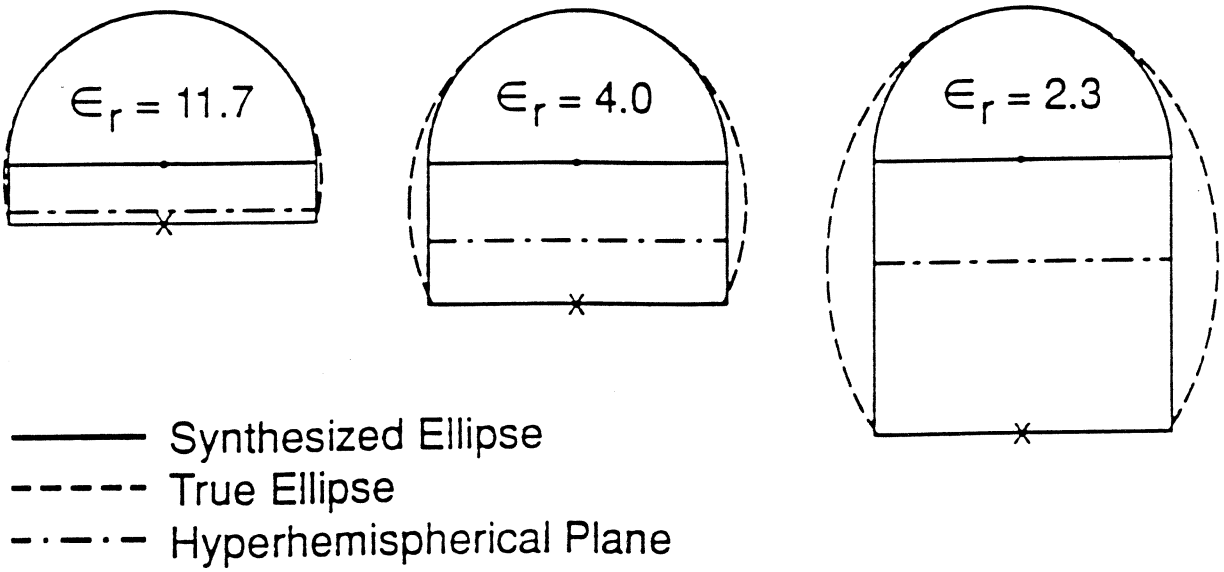

Figure 2: The synthesis of an elliptical lens from a hyperhemispherical lens and planar wafers. The extended hemisphere is a very good geometrical approximation to an elliptical lens at high dielectric constants.

where $k_e = k_{diel} = 2\pi/\lambda_{diel}$ for the dielectric side, $k_e = 2\pi/\lambda_{air}$ for the air side, and θ is the angle with respect to the z-axis. The element pattern is a constant in the E-plane. The E-plane array factor is given by:

$$\cos(k_e d \sin\theta \cos\phi) \tag{7}$$

where ϕ is the angle from the x-axis in the x-y plane, k_e is defined as above, and d is the spacing between the two slots.

Figure 3 shows the calculated radiation patterns at 246GHz of a double-slot antenna with length $l = 0.28\lambda_{air}$ and spacing $d = 0.16\lambda_{air}$ into a dielectric with a relative dielectric constant of $\epsilon_r = 11.7$. The double-slot antenna results in symmetrical patterns in the infinite dielectric half space with a -10dB beamwidth of around 48° and a cross-polarization level lower than -30dB in the 45°-plane. The phase is constant across the main-beam, and the power radiated in the main-beam illuminates the whole spherical surface of the extended hemispherical lenses considered in this paper. The patterns radiated to the air-side are broader with a -10dB beamwidth of 70° in the H-plane and a nearly uniform E-plane, and contain 9.0% of the radiated power.

The radiation patterns from the extended hemispherical lenses are computed using a ray-tracing technique [23]. The double-slot antenna patterns into the dielectric are used to calculate the distribution of the electric and magnetic fields across the spherical surface of the extended hemispherical lenses (Fig. 1). It is important to note that this analysis is not limited to double-slot antennas and is applicable to any planar antenna designed to yield similar patterns in the dielectric; for example, the double-dipole and spiral/log-periodic antennas. For a given ray, the fields are decomposed into parallel/perpendicular components at the lens/air interface, and the appropriate transmission formulas are used for each mode [24]:

$$\Gamma_{\|} = \frac{n\sqrt{1 - n^2\sin^2\theta_i} - \cos\theta_i}{n\sqrt{1 - n^2\sin^2\theta_i} + \cos\theta_i} \tag{8}$$

$$\tau_{\|} = (1 + \Gamma_{\|})\frac{\cos\theta_i}{\sqrt{1 - n^2\sin^2\theta_i}} \tag{9}$$

$$\Gamma_{\perp} = \frac{n\cos\theta_i - \sqrt{1 - n^2\sin^2\theta_i}}{n\cos\theta_i + \sqrt{1 - n^2\sin^2\theta_i}} \tag{10}$$

$$\tau_{\perp} = 1 + \Gamma_{\perp} \tag{11}$$

where n is the dielectric constant, θ_i is the angle of incidence from the normal to the spherical lens (Fig. 1), and Γ and τ are the reflection and transmission coefficients for the parallel ($\|$) and perpendicular ($\perp$) polarizations. Once the electric and magnetic fields have been found, equivalent electric and magnetic current densities [24] are calculated just outside the spherical surface using:

$$\mathbf{J}_S = \hat{n} \times \mathbf{H} \tag{12}$$

$$\mathbf{M}_S = -\hat{n} \times \mathbf{E} \tag{13}$$

where $\hat{n}$ is the normal to the interface, and $\hat{n} = \hat{a}_r$ when the origin of the coordinate system is defined to be the center of the spherical surface. In the far-field, the transverse electric field is equal to:

$$\mathbf{E}_\theta \cong -\frac{jke^{-jkr}}{4\pi r}(\mathbf{L}_\phi + \eta \mathbf{N}_\theta) \tag{14}$$

$$\mathbf{E}_\phi \cong +\frac{jke^{-jkr}}{4\pi r}(\mathbf{L}_\theta - \eta \mathbf{N}_\phi) \tag{15}$$

where $\mathbf{N}$ and $\mathbf{L}$ are defined by:

$$\mathbf{N} = \iint_S \mathbf{J_S} e^{jkr'\cos\psi} ds' \tag{16}$$

$$\mathbf{L} = \iint_S \mathbf{M_S} e^{jkr'\cos\psi} ds' \tag{17}$$

where s' is the closed surface just outside the lens, r' is the distance from the origin of the coordinate system to the equivalent electric and magnetic currents, r is the distance from the origin to the far-field point, and ψ is the angle between r and r'. A matching layer at the lens/air interface is not yet considered in this analysis.

The computed E and H-plane power patterns and the phases of the electric field in the E-plane of a 13.7mm diameter lens fed by a double-slot antenna at 246GHz are shown for extension lengths of 1600μm, 1800μm, 2000μm, 2200μm, 2400μm, 2600μm, 2800μm, and 3000μm (Fig. 4). It is seen that the patterns become progressively narrower resulting in higher directivity up to 2600μm and then the mainlobe widens and the sidelobe levels begin to increase. It is important to note that the phase of the field is not constant in the mainlobe except around the synthesized elliptical position (determined to be L = 2670μm). This is seen on the 2600μm plot where the phase is nearly constant in the mainlobe and then shifts 180° in the first sidelobe. The corresponding peak directivity and the Gaussicity (pattern coupling efficiency) as a function of the extension length are shown in Figure 5. The Gaussicity is computed using an overlap integral between the far-field patterns and the far-field Gaussian-beam expression (see Appendix). The directivity has a broad peak of 30.2dB centered at L_{pk} = 2550μm and remains within 1.0dB of the peak between 2400μm and 2800μm. The corresponding aperture efficiency (coupling to a plane wave) peaks at 84% and is above 68% between 2400μm and 2800μm. This peak position agrees well with Büttgenbach's formulation on the diffraction-limit of a lens (see [19] for more detail). In the far-field, the decrease in Gaussicity at the larger extension lengths can be interpreted as the result of the formation of out-of-phase sidelobes whose level progressively increases as the extension length is increased. It is seen that the Gaussicity is very high up to 2200μm (above 95%) and drops to 88-86% at the peak directivity and synthesized elliptical positions.

The near-field waist and radius of curvature are found from an inverse Fourier transform of the far-field Gaussian-beam [23] (Fig. 6). These are referenced to the aperture plane at the tip of the lens (Fig. 1). As expected, the radius of curvature is infinity at the synthesized elliptical position (L = 2670μm) and changes sign immediately afterwards. This means that the synthesized elliptical lens is a good approximation to a true elliptical lens

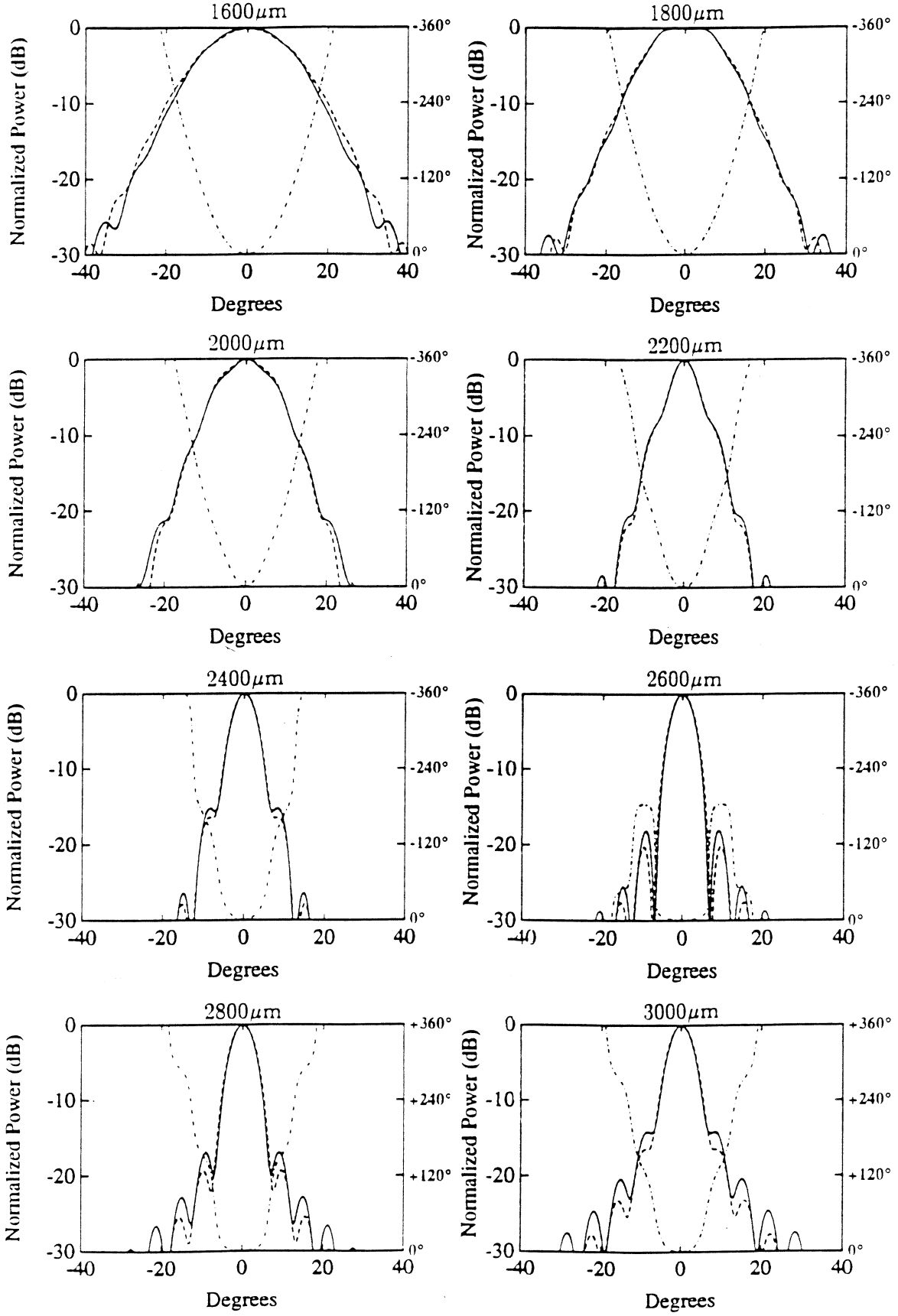

Figure 4: E and H-Plane power patterns and phase in the E-plane at 246GHz for extension lengths of 1600μm, 1800μm, 2000μm, 2200μm, 2400μm, 2600μm, 2800μm, and 3000μm The dashed/dotted line corresponds to the phase.

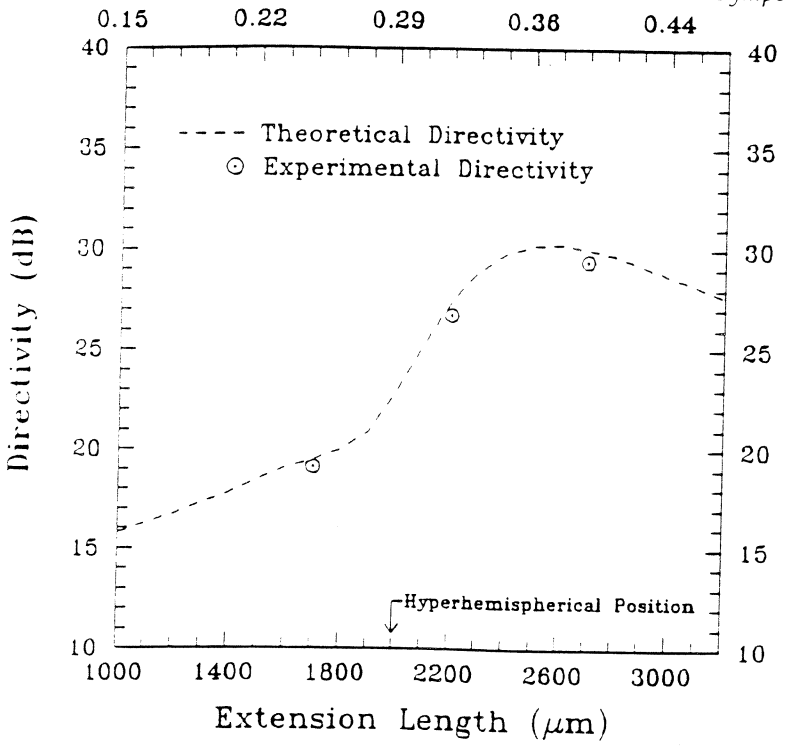

Figure 5: Directivity and maximum Gaussian-coupling efficiency as a function of extension length at 246GHz (see text).

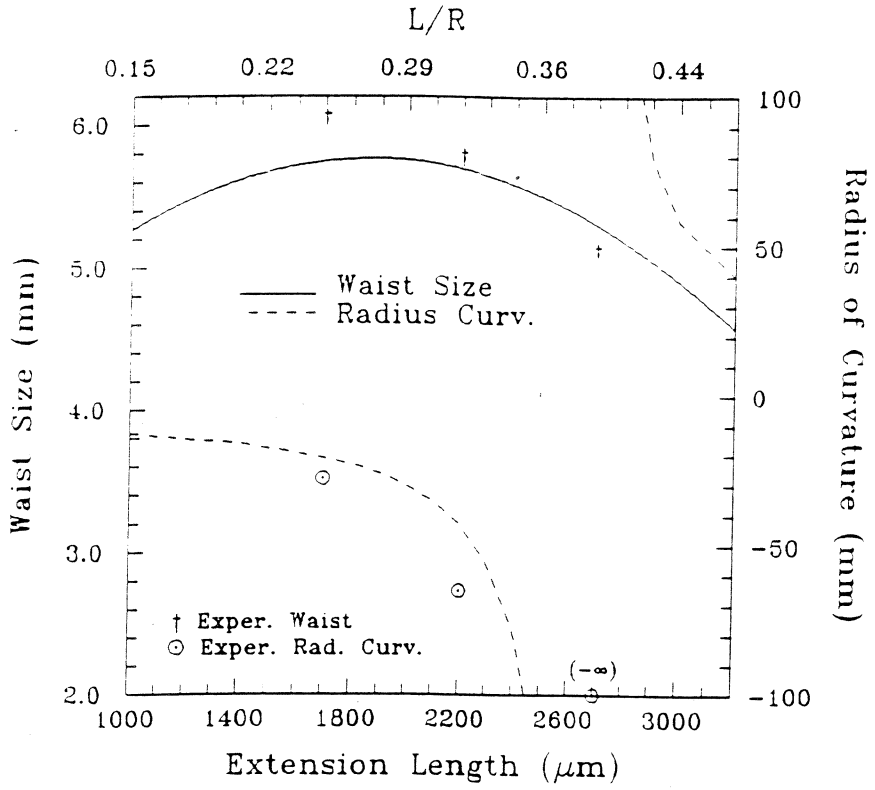

Figure 6: Waist and radius of curvature as a function of the extension length at 246GHz (see text).

and couples best to a Gaussian-beam at its minimum waist. The Gaussian-beam radius of curvature approaches the lens radius (6.858mm) when the extension length is small, as expected. The beam waist is nearly constant at 5.6±0.3mm for extension lengths between 1000μm and 2700μm and 5.8±0.1mm between 1800μm and 2300μm. It is mainly the radius of curvature that is changing from -13mm to -∞ between 1000μm and 2700μm. Therefore, the converging Gaussian-beam must be very well characterized on the lens aperture for optimal Gaussian-coupling efficiency.

In order to gain a more intuitive understanding of the optimal radius of curvature, the phase of the electric field on the aperture plane is presented in Fig. 7 for the lens system at 246GHz. The phase is calculated using a ray-optics approach all the way to the aperture-plane. This method has proven to result in a caustic with the extended lens system and is not used for far-field pattern and Gaussian-beam calculations (a caustic is a region where an infinite number of rays converge and therefore results in a singularity). However, the method does yield a physical understanding of the problem. The phase of the electric fields on the planar aperture is seen to follow a near quadratic behaviour with varying curvature depending on the extension length. For larger extension lengths (L = 2200μm and above) the phase is plotted up to the caustic region. For low extension lengths, the aperture fields extend significantly beyond the diameter of the lens due to the weak refraction of the wide angle rays, and this contributes to the high Gaussicity. This is not shown in Figure 7 since the phase is only plotted to 180°. At L = 2700μm (just near the synthesized elliptical postion) the phase is nearly constant, and then begins to increase positively for increasing extension length.

A similar analysis of a 13.7mm diameter lens was performed at 100GHz and 500GHz, assuming the same radiation patterns of the feed antenna. Figure 8 shows the patterns and phases for extension lengths of 1600μm, 1800μm, 2000μm, 2200μm, 2400μm, 2600μm, 2800μm, and 3000μm at 500GHz. The directivity and Gaussicity calculations at 100GHz, 246GHz and 500GHz are shown in Figure 9. The corresponding waists and radii of curvature are shown in Figure 10. At 100GHz, the peak in the directivity curve occurs at 2480μm and is very broad. The corresponding Gaussicity is very smooth with a drop of 10% at the synthesized elliptical position. On the other hand, at 500GHz, the directivity curve shows a distinct peak of 36.3dB centered at 2600μm (with a corresponding aperture efficiency of 72%) and drops by 0.5dB at the synthesized elliptical position. Again, this position agrees well with Büttgenbach's diffraction method (see [19] for more detail). Note that at higher frequencies, the peak directivity is closer to the synthesized elliptical position, which is the result of the geometrical optics approximation becoming more accurate. The Gaussicity peaks at 500GHz at the hyperhemispherical position of 2000μm with a value of 97% and then drops to 82% at the 2600μm-2700μm position. Again, as the frequency increases, the ray-optics approximation becomes more valid, and this explains the peak in Gaussicity at the hyperhemispherical position.

The directivity and Gaussicity are calculated for a true elliptical lens using the same approach for the extended hemispherical lens at 246GHz. The true elliptical lens is defined such that the minor axis (perpendicular to boresight) is equal to the radius of the extended

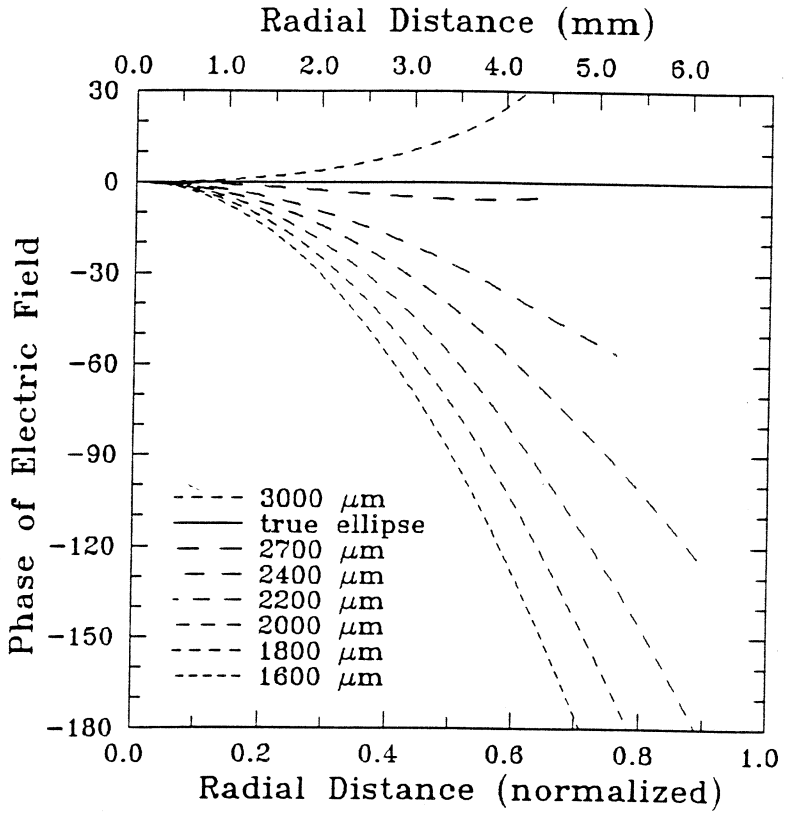

Figure 7: Phase of the aperture electric field at 246GHz for extended hemispherical lenses with different extension lengths with the double-slot antenna as the feed.

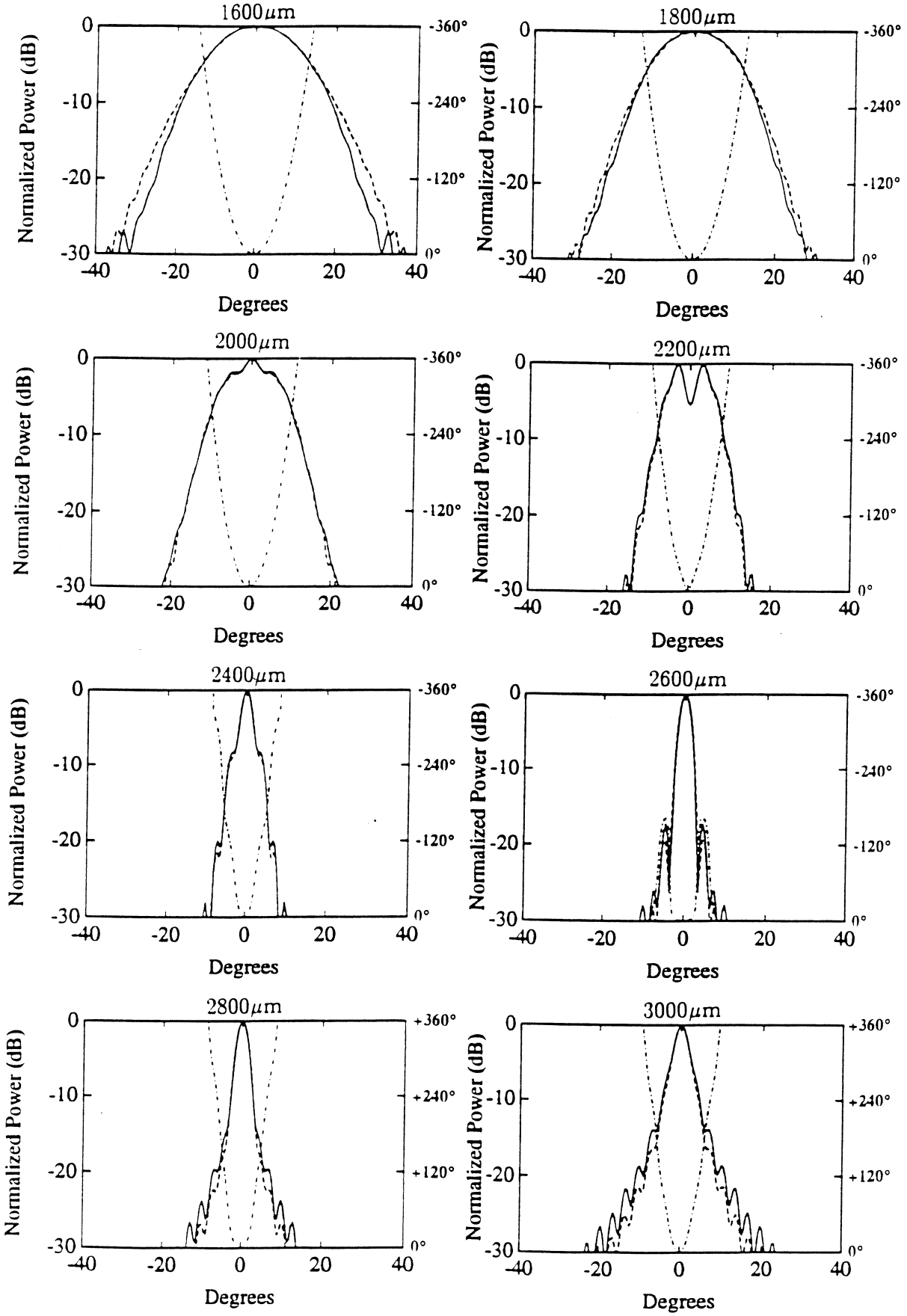

Figure 8: E and H-Plane power patterns and phase in the E-plane at 500GHz for extension lengths of 1600μm, 1800μm, 2000μm, 2200μm, 2400μm, 2600μm, 2800μm, and 3000μm. The dashed/dotted line corresponds to the phase.

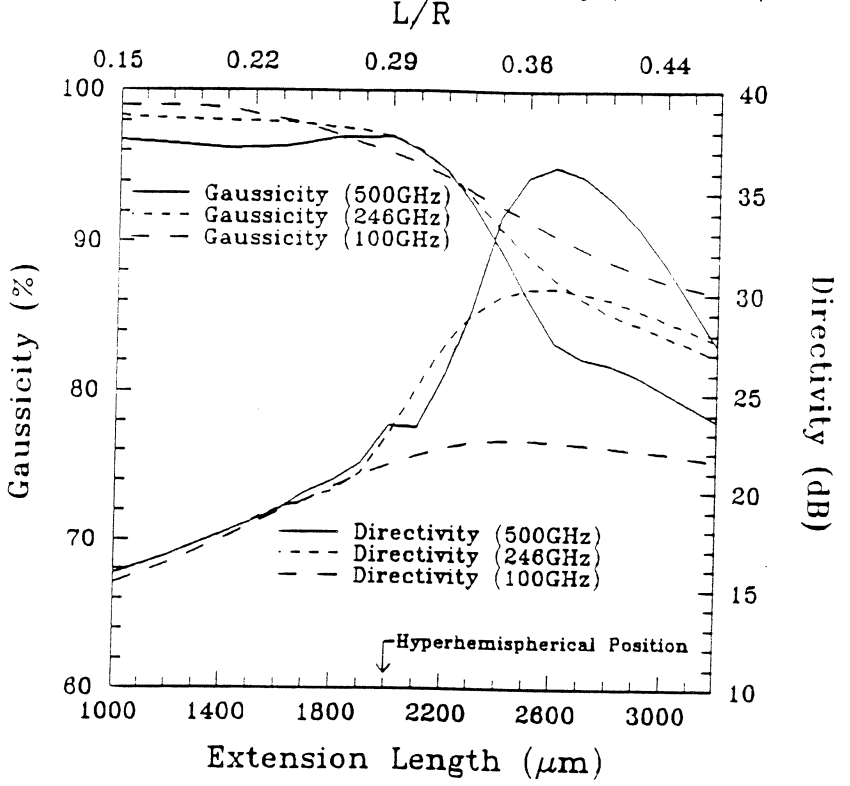

Figure 9: Directivity and maximum Gaussian-coupling efficiency as a function of extension length at 100GHz, 246GHz, and 500GHz (see text).

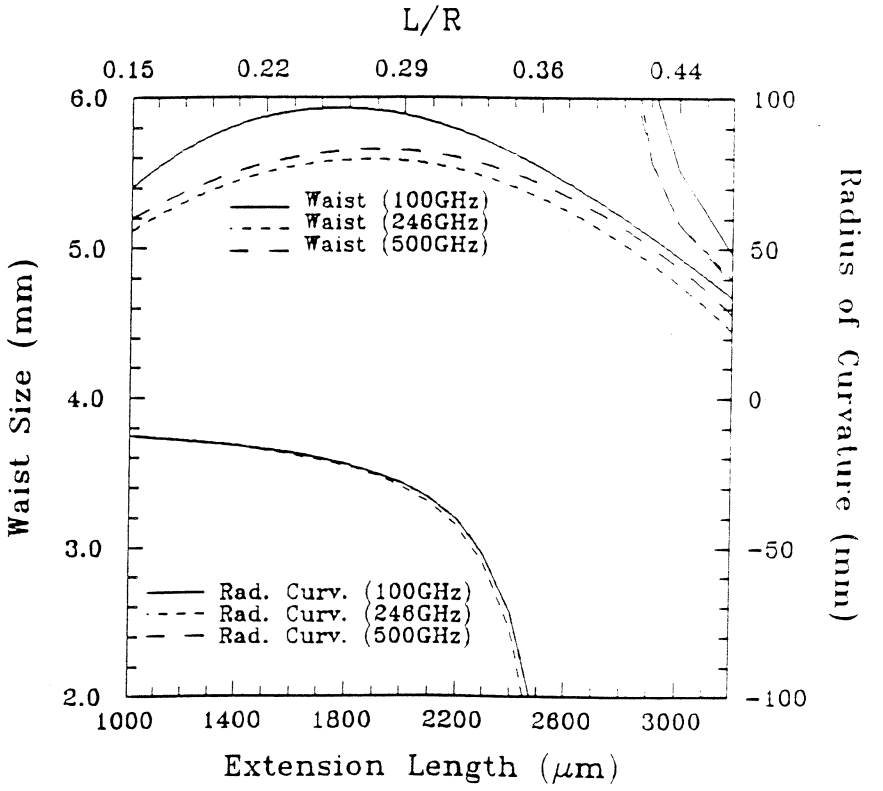

Figure 10: Waist and radius of curvature as a function of extension length at 100GHz, 246GHz, and 500GHz (see text).

hemispherical lens, so that the physical area on the aperture plane is the same for both lenses. The E and H-plane mainlobes are slightly narrower than those of the synthesized elliptical lens and have 0.5dB higher sidelobes. The directivity is 30.6dB which is 0.6dB higher than the synthesized ellipse. The elliptical lens Gaussicity is 88% and is the same to within ±1% for the synthesized elliptical lens. The corresponding minimum waist at the aperture plane is 5.6mm.

IV. REFLECTION LOSS CALCULATIONS

The ray-tracing technique presented earlier (Fig. 1) also results in a full characterization of the reflection loss at the lens-air interface as a function of the extension length (Figure 11). The reflection loss is calculated by using equations 8 and 10 and integrating the reflected power over the entire surface of the lens. At low extension lengths, the calculated loss is 1.52dB which is close to the 1.55dB predicted from simple transmission-line theory (between silicon and air). The reflection loss increases to 2.1dB at the synthesized elliptical position (L = 2670μm) due to the power loss from the total internal reflection of wide angle rays (above 65°). The Gaussian-coupling efficiency of the extended hemispherical system must include the reflection loss to result in a complete characterization of the system. This results in an *additional* decrease of 13% in the Gaussian-coupling efficiency at the synthesized elliptical positions compared to the Gaussian-coupling efficiency at the hyperhemispherical position. The calculated reflection loss at the synthesized elliptical position is 1.8dB for an antenna with a symmetrical pattern and a 10dB-beamwidth of 46° (corresponding to a directivity of 12dB) and a nearly constant 1.52dB for antennas with a 10dB-beamwidth of 40° and 31° (corresponding to a directivity of 13dB and 15dB). This means that it is advantageous to use a high gain antenna for a feed into the extended hemispherical lens. This is important at high frequencies (above 300GHz) where it may be difficult to manufacture an accurate matching layer for the silicon lens. While it is not known accurately, it is expected that the spiral antenna [19] and log-periodic antenna [13] have a pattern directivity into the lens of around 12dB. As expected, the calculated reflection loss of an elliptical lens is nearly equal to the reflection loss at the sythesized elliptical position.

Figure 11 also includes the reflection loss using a $\lambda_m/4$ matching cap layer with dielectric constant equal to $\sqrt{\epsilon_{lens}}$. The reflection loss for the double-slot antenna (directivity=11.1dB) is nearly zero up to the hyperhemispherical position, and then increases to 0.6dB at the synthesized elliptical position. The radiation patterns and the directivities remain essentially the same with the matching cap layer. As expected, the reflection loss for the higher directivity antennas are lower with a loss of 0.3dB, 0.1dB, and zero for the 12dB, 13dB, and 15dB pattern directivities at the synthesized elliptical position. No attempt is made in this paper to design an optimum matching layer (i.e. non-uniform) for the higher extension lengths.

V. GAUSSICITY VS. FREQUENCY

A comparison of the directivity and Gaussicity between the true elliptical lens, the synthesized elliptical lens, and an extended hemispherical lens at peak directivity position for

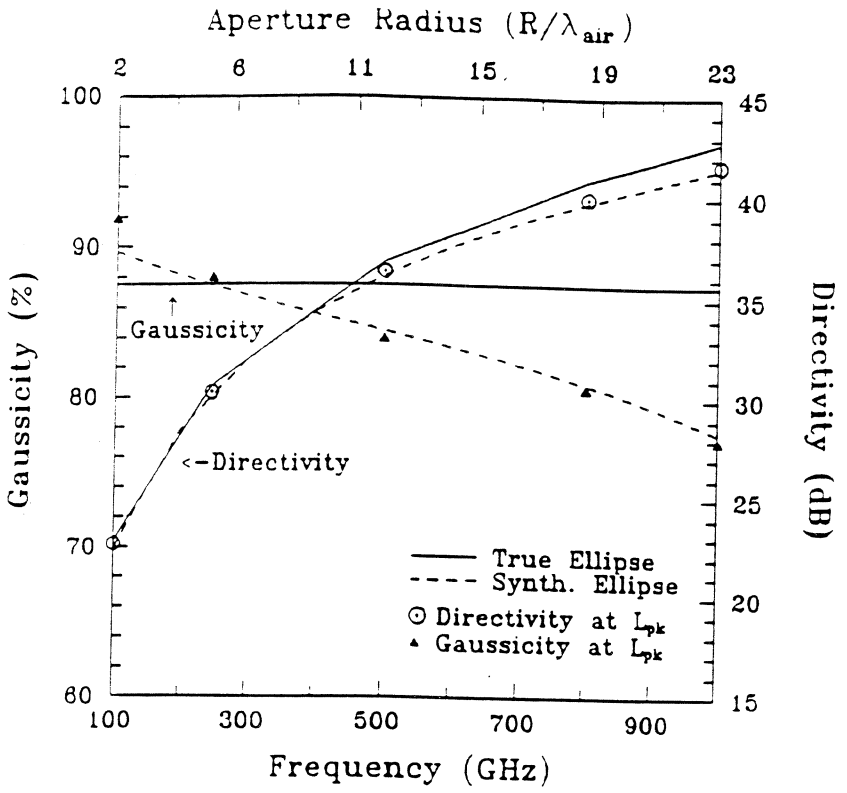

Figure 11: Reflection loss at the lens/air interface as a function of the extension length for different feed antenna directivities with and without a matching layer.

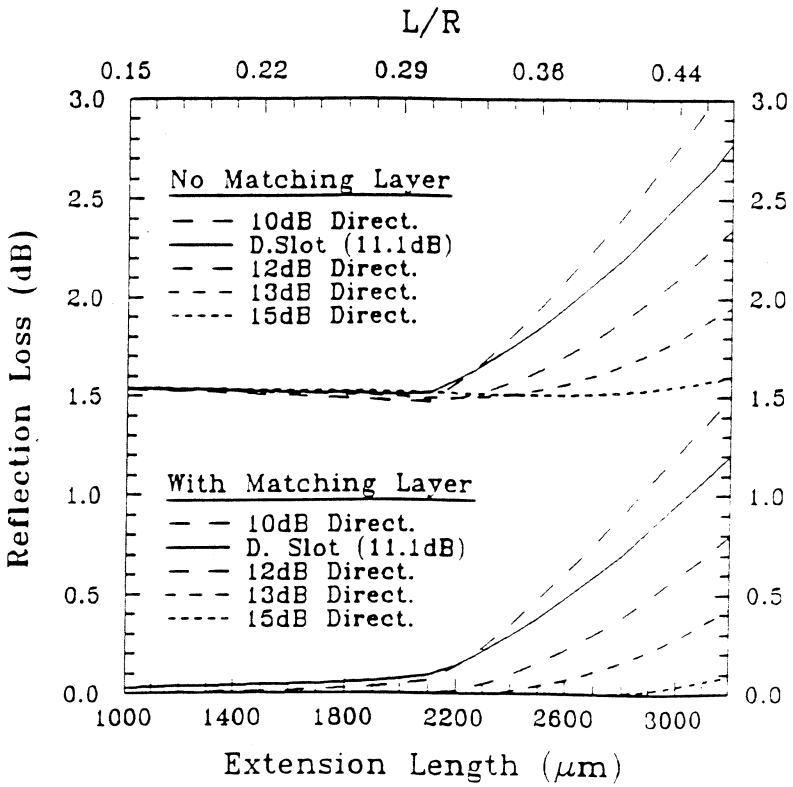

Figure 12: Directivity and maximum Gaussicity (pattern coupling efficiency) as a function of frequency (or lens radius) for a true elliptical lens, a synthesized elliptical lens, and an extended hemispherical lens at peak directivity position (L_{pk}).

100GHz-1THz is shown in Fig. 12. The true elliptical lens has a constant Gaussicity of 88% and a quadratic increase in the directivity, as expected from ray-optics calculations. The directivity of the synthesized elliptical lens shows a 1.2dB drop compared to the elliptical lens at 1THz due to the residual phase error on the planar aperture. The Gaussicity drops from about 90% at 100GHz to 78% at 1THz due to the same effect. As was seen in Fig. 9 at 246GHz and 500GHz, there exists a distinct peak in the directivity at a specific extension length (L_{pk}). Figure 13 shows that L_{pk} asymptotically approaches the synthesized elliptical position with increasing radius/wavelength (or increasing frequency for a constant radius). The peak directivity is slightly higher than the synthesized elliptical directivity and is nearly the same above 500GHz. The Gaussicities for peak directivity positions are the same as those of the synthesized elliptical position to within $\pm 1\%$ above 200GHz. At 100GHz, the peak directivity position is close to the hyperhemispherical position, and therefore results in a slightly larger Gaussicity.

The Gaussicity and directivity for extension lengths of 2000μm, 2350μm, and 2700μm are shown in Figure 14. The hyperhemispherical lens results in a constant directivity of 22dB and a constant Gaussicity of 97%. Notice that the directivity is constant with freqency due to the constant n^2 magnification of the hyperhemispherical lens. The Gaussicity at 2350μm is slightly lower than the hyperhemispherical lens and the directivity increases to around 30dB at high frequencies. The Gaussicity at 2700μm (close to the synthesized elliptical position) is the lowest of all three positions, but results in the largest directivity. The Gaussicity at the synthesized elliptical position (and at L_{pk}) drops to 78% at 1THz while the Gaussicity for the 2350μm position drops to 88% at the same frequency. Although the hyperhemispherical position shows the highest theoretical Gaussicity, it is hard to experimentally achieve this efficiency due to the difficulty in aligning to the strongly converging beams needed at the aperture of the lens (see section VII). Thus the region between 2200μm and 2400μm results in the best compromise between alignment, directivity and Gaussian-coupling efficiency.

Since all the calculations were done in terms of wavelength, Figures 12 and 14 present universal design curves to predict the performance of extended hemipsherical silicon lenses for different diameters when using the same antenna feed patterns. These graphs shows that for high gain systems, a 13.7mm diameter silicon lens can be used in an extended hemispherical configuration up to 1THz without a significant drop in the Gaussicity. For a matched load, the Gaussian-coupling efficiency is found by multiplying the Gaussicity presented above by the reflection loss at the lens-air interface (shown in Figure 11) and by 91.0% to take into account the power radiated by the double-slot antenna to the back-side (air-side). It is important to note that the reflection loss for higher extension lengths (near L_{pk} and the synthesized elliptical position) will have an *additional* loss of about 0.5dB (10%) over the hyperhemispherical position (2000μm).

VI. EXPERIMENTAL RESULTS: PATTERNS

The double-slot antenna was fabricated for 246GHz measurements using standard photolithographic techniques. All the conducting layers are 2000Å gold deposited on a high-resistivity ($4000\Omega - \text{cm}$) silicon wafer. A bismuth bolometer is placed in series at the center of the double-slot antenna using a coplanar-waveguide transmission line (Fig. 3). The series

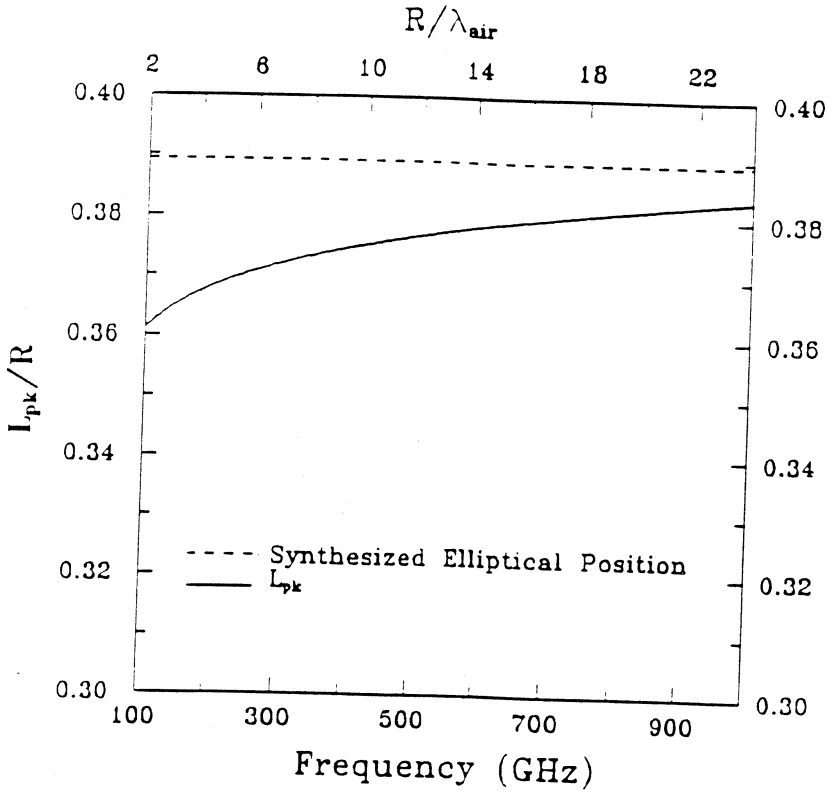

Figure 13: Extension length for peak directivity versus frequency (or R/λ).

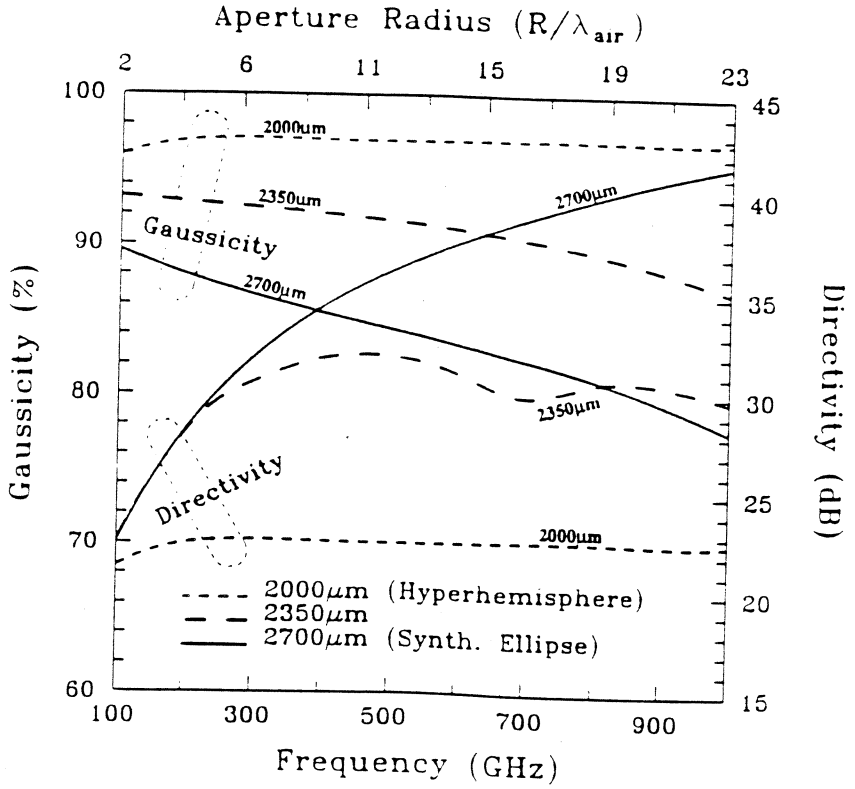

Figure 14: Directivity and Gaussicity (pattern coupling efficiency) as a function of frequency (or lens radius) for an extended hemispherical lens at L=2000μm, 2350μm, and 2700μm.

feeding is necessary in order to result in the sum mode of the double-slot antenna. The bolometer is 20μm x 15μm and is integrated on a 1.2μm thick polyimide patch for thermal insulation from the substrate. The measured DC resistance of the bolometer is 60Ω. The left and right ends of the coplanar line are terminated by a polyimide/gold capacitor which acts as an RF short. The center strip of the coplanar waveguide line runs out from the right end to a large pad for DC biasing and low frequency detection. The coplanar waveguide spacing is 15μm and the width 10μm. This yields a quasi-TEM transmission line impedance of 50Ω [25]. The measured RF impedance at the bolometer position is $60 + j50\Omega$ on a 4GHz microwave model, and results in a good match to the bolometer.

Experimental measurements at 246GHz were performed on a 13.7mm diameter silicon lens (ϵ_r=11.7) without any type of matching layer and the double-slot antenna as a feed. Three particular values of extension length were chosen for the purpose of experimental verification: 1700μm, 2200μm, and 2700μm. The extension lengths were achieved by adding high-resistivity silicon wafers. These positions were chosen based on their different properties: a phase curvature across their aperture planes of high, low, and virtually none, respectively; and a radiation pattern that is broad, narrow with nearly no sidelobes, and narrow with low sidelobes, respectively. The position of 2700μm represents the extension length where the extended hemispherical lens has effectively synthesized an elliptical lens. The hyperhemispherical position is at 2000μm and no measurements were done at this position. However, the 1700μm extension has the same features as the 2000μm position in terms of Gaussian-coupling efficiency and the small radius of curvature needed to couple well to a Gaussian-beam. No pattern measurements were done on a true elliptical lens.

The patterns were measured at 246GHz using an 82GHz Gunn source, and a wideband (220-270 GHz) tripler. The Gunn source was modulated at 1040Hz, and the output from the bolometer was fed to a lock-in amplifier. Measured patterns at the extension length of 2700μm (Fig. 15) demonstrate a directivity of 29.4dB$\pm$0.3dB with relatively low sidelobes (-16dB). The corresponding aperture efficiency (coupling to a plane wave) is 70%$\pm$5%. Notice that the theoretical analysis predicts a directivity of 29.9dB (78% aperture efficiency) at the synthesized elliptical position. Good agreement exists between the theoretical and experimental patterns (Fig. 16). Measured patterns at 2700μm for $\pm$10% of the 246GHz design frequency result in nearly the same directivity, and therefore the double-slot antenna has good pattern bandwidth. The measured power at broadside is nearly the same from 222GHz-270GHz, also indicating good impedance bandwidth for the double-slot design. The measured patterns at an extension length of 2200μm are slightly broader than the synthesized elliptical lens with a directivity of 26.7dB$\pm$0.3dB. Again, there is close agreement between theory and experiment (Fig. 17). At an extension length of 1700μm, the patterns become wide with a peak gain of 19.1dB$\pm$0.3dB, and it is considerably more difficult to laterally align the feed antenna to the focus, resulting in non-symmetric patterns with ripples (Fig. 18). As was seen earlier, this wide pattern has no detrimental effect on the coupling efficiency to a converging beam. The ratio of the 246GHz measured peak received power between the extension lengths of 2700μm and 1700μm is 10dB$\pm$0.5dB and this is the same as the difference in the measured directivities (including the effect of the different reflection losses at the lens surface).

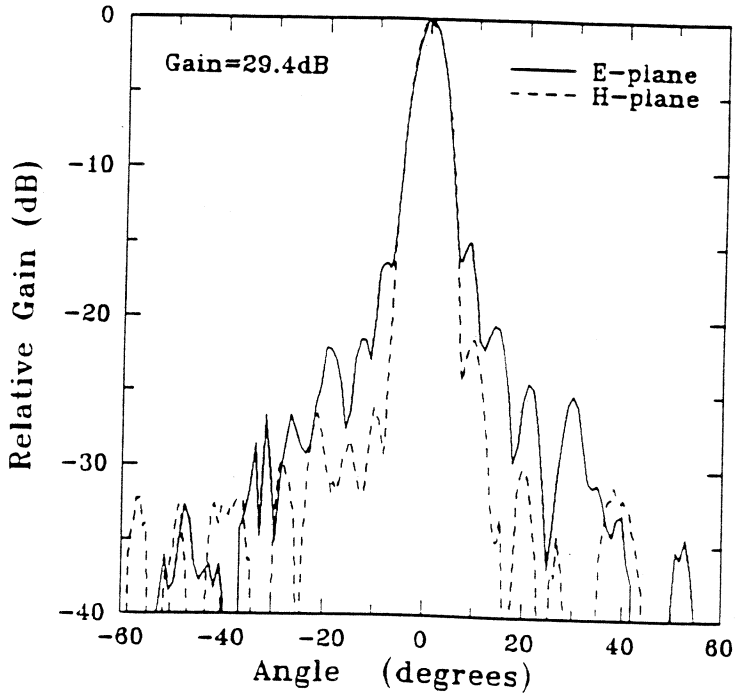

Figure 15: Measured patterns for the synthesized elliptical lens (2700μm) at 246GHz. The patterns are diffraction-limited by the size of the aperture. The S/N ratio is better than 40dB.

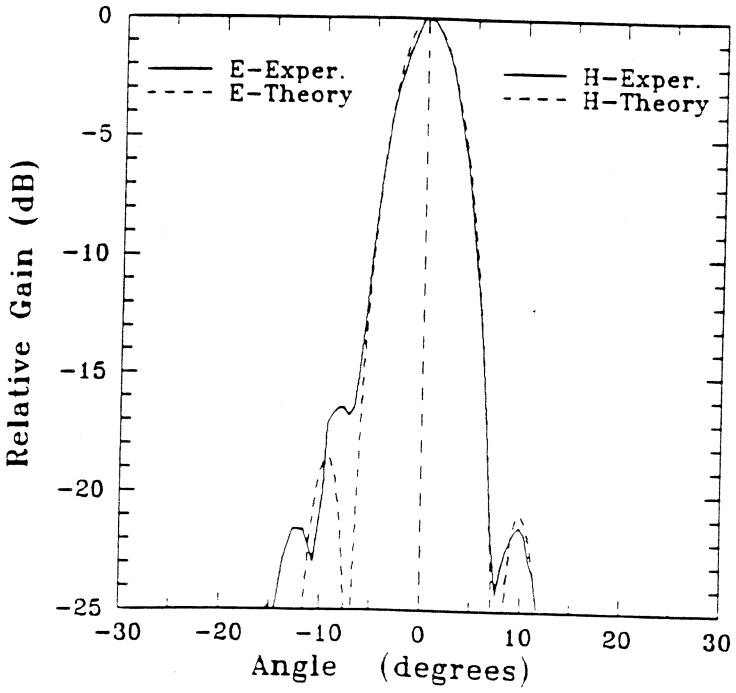

Figure 16: Comparison of the calculated patterns versus experiment at 246GHz for the double-slot antenna on a synthesized elliptical lens (extension length 2700μm).

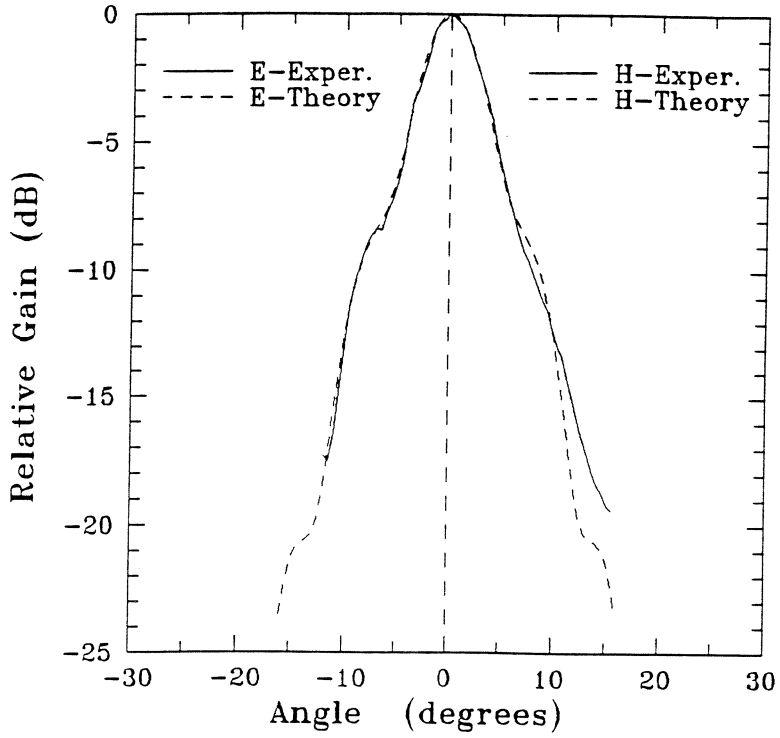

Figure 17: Comparison of the calculated patterns versus experiment at 246GHz for the double-slot antenna on an extended hemispherical lens with 2200μm extension length.

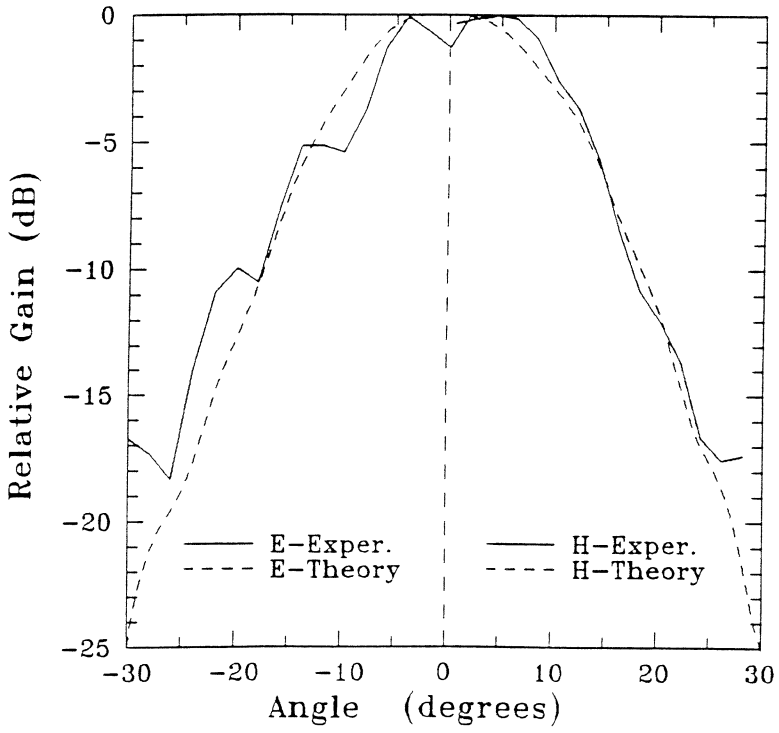

Figure 18: Comparison of the calculated patterns versus experiment at 246GHz for the double-slot antenna on an extended hemispherical lens with 1700μm extension length.

VII. EXPERIMENTAL RESULTS: GAUSSIAN-BEAM COUPLING

A Gaussian-beam experiment was performed at 246GHz with the purpose of coupling all the power radiated by a corrugated horn into the double-slot antenna/lens system. A two-lens quasi-optical system was designed which achieves a wide variety of waist sizes and radii of curvature (Fig. 19). The 10-cm Rexolite lenses used were numerically machined using parametric equations and result in no spherical aberrations [26]. The source was a WR-03 corrugated horn having symmetric E, H, and 45° patterns with a computed waist size of $w_0 = 2.1$mm. The waist can be traced through the lens system using the q-parameters [27]. In Figure 19, d1, d2, and d3 are the lens seperation distances, and f_1 and f_2 are the respective $f/\#$'s ($f/\#$ = f/D, where f is the focal length and D is the diameter of the lens). Care must be taken that the edge illumination of the lens is below the -30dB level so that the Gaussian-beam does not deform from its ideal shape. The experimental procedure went as follows: the distances d1, d2, and d3 and the $f/\#$'s f_1 and f_2 were first calculated for maximum coupling between the corrugated horn and the extended hemispherical lens system. Then, the distances d1, d2, and d3 were tuned experimentally to result in peak measured power in the bolometer.

2700μm extension length (synthesized ellipse): An equiphase wavefront is needed for the synthesized ellipse and is obtained at the minimum waist. A quasi-optical system with final values of $d_1 = 96$mm, $d_2 = 68$mm, $d_3 = 312$mm, $f_1/2.0$, and $f_2/1.4$ resulted in a peak received power with a calculated minimum beam-waist of 5.1mm at the planar lens aperture. The beam waist for optimum Gaussicity calculated from the present theory is 5.2mm. The final values of d1, d2, and d3 are within $\pm$1mm of the initially calculated values.

2200μm extension length: A quasi-optical system with final values of $d_1 = 95$mm, $d_2 = 122$mm, $d_3 = 224$mm, $f_1/2.0$, and $f_2/1.4$ resulted in peak received power. The calculated beam waist and radius of curvature were 5.78mm and -65mm, respectively. The corresponding minimum waist is 2.8λ and is located -35mm (away from the horn) from the aperture plane. The final values of d1, d2, and d3 are within $\pm$5mm of the initially calculated values.

1700μm extension length: A quasi-optical system with $d_1 = 106$mm, $d_2 = 120$mm, $d_3 = 86$mm, $f_1/0.9$, and $f_2/2.0$ resulted in peak received power. The calculated beam waist and radius of curvature were 6.07mm and -27.7mm, respectively. The corresponding minimum waist is 1.1λ (a result of the small radius of curvature necessary at the aperture of the lens). The final values of d1, d2, and d3 differ by as much as $\pm$25mm to the initially calculated values. We believe that for this extension length, the radius of curvature across the aperture is so strong that the desired aperture field distribution will distort rapidly with misalignments of the feed antenna to the lens. This is commonly seen in optics where it is difficult to align to a lens system with small f/D ratios.

The raw measured powers were 1.03, 1.18 and 1.00 for the 1700μm, 2200μm, and 2700μm positions, respectively. In the experimental setup, the 2200μm and 2700μm systems used the same set of objective lenses ($f_1/2.0$ and $f_2/1.4$) and therefore have approximately the same reflection and dielectric losses in those lenses. The 1700μm experiment required $f_1/0.9$ and $f_2/2.0$ lenses and has approximately an additional 6-10% loss due to the added

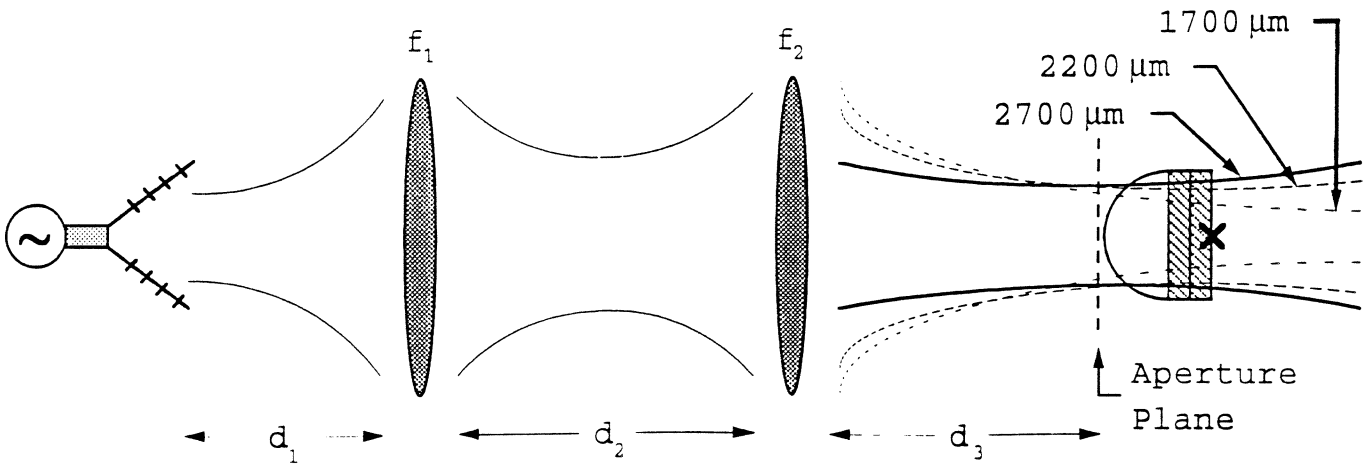

Figure 19: The setup for the Gaussian-beam coupling experiment. The waist at the aperture is 5.2-5.9mm for all three lenses, and only the radii of curvature are different.

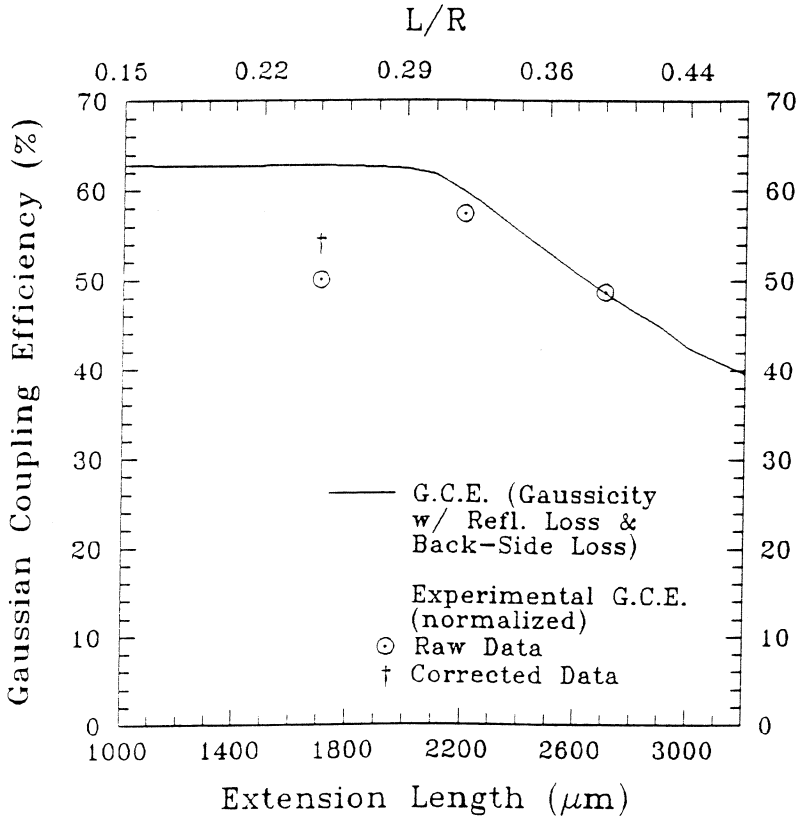

Figure 20: Measured and calculated Gaussian-coupling efficiency as a function of extension length. This takes into account reflection at the lens/air interface and power lost to the air side (91%).

thickness of the $f/0.9$ lens. The measured power at the 1700μm position is therefore multiplied by 1.08 to take into account the excess dielectric loss for the 1700μm quasi-optical system, resulting in a corrected power of 1.11 (shown as a cross in Fig. 20). The theoretical Gaussicities are multiplied by the different reflection losses at the silicon-air interface (see Fig. 11) for the three lens systems, and by the back-side power loss (91%) to yield the actual Gaussian-coupling efficiency. The theoretical Gaussian-coupling efficiencies are presented in Figure 20, together with the measured powers which have been normalized to the 2700μm position. This position was chosen for the normalization because the experimental waist and radius of curvature at 2700μm agree very well with the theoretical values. The normalization is necessary since no absolute power measurements were done at 246GHz. It is seen that within experimental error, the measured values agree well with the theoretical predictions at extension lengths of 2200μm and 2700μm. Notice that the 2700μm position results in the lowest measured Gaussian-coupling efficiency. Also, the measured Gaussian-coupling efficiency at 2200μm is 7% and 18% higher than the measured Gaussian-coupling efficiencies for the 1700μm and 2700μm positions, respectively. This agrees well with our calculations in section V which state that the 2200μm-2400μm positions (L/R= 0.32 to 0.35) result in the best compromise between directivity and Gaussian-coupling efficiency.

VIII. DISCUSSION AND CONCLUSION

In this paper, a ray-optics/field-integration approach has been used to fully characterize an extended hemispherical lens system with a double-slot antenna feed. We have also presented a formulation for synthesizing an ellipse from an extended hemispherical lens. The results show that the directivity is strongly dependent on the extension length (especially at high frequencies). The calculated Gaussicity (pattern coupling efficiency) is very high up to approximately 2200μm and then drops gradually by about 10-15% at the synthesized elliptical position (depending on frequency). The corresponding beam waist on the aperture-plane is nearly constant (5.6$\pm$0.3mm) and the radius of curvature ranges from -13mm to -∞. Thus the incident Gaussian-beam must be very well characterized on the planar aperture for optimum coupling efficiency. In fact, we have built a lens system with a 10dB difference in directivity and still succeeded in achieving nearly the same Gaussian-coupling efficiency for the low and high directivity systems. Our calculations also show that a 13.7mm diameter silicon lens can be used up to about 1THz without a significant drop in the Gaussian-coupling efficiency (maximum 20%) and has an associated directivity greater than 40dB. The Gaussian-coupling efficiency for a double-slot antenna at a position between 2200μm to 2400μm (L/R= 0.32 to 0.35) is approximately 60-50%, which includes the reflection loss and the back-side power loss. This is expected to increase to about 90-80% when a matching cap layer is used.

The question arises of where to place the antenna on a lens for the best possible performance. The answer, according to our calculations, depends on the specific application (for example, a single unit or a unit in an imaging array). For *single units*, the hyperhemispherical position is not the best place since it results in a low directivity, and requires small $f/\#$ systems that are difficult to align. This was well demonstrated by our quasi-optical set-up and we found that it was very difficult to choose the position of the lenses for best

Gaussian-coupling efficiency at the 1700μm extension length. In our opinion, one should use an extension length that results in an acceptably high directivity and therefore a large $f/\#$ for the objective lens. This also yields an easy-to-align quasi-optical system. However, the high directivity is achieved at the expense of a reduction in the Gaussian-coupling efficiency. For a 13.7mm diameter silicon lens, we believe that a good compromise between the increase in directivity and the decrease in Gaussian-coupling efficiency is achieved at 2200μm-2400μm extension length (L/R= 0.32 to 0.35). The corresponding Gaussicity is very high being always above 90% for frequencies below 1THz. This was well demonstrated in our experimental setup at 246GHz where the 2200μm positions resulted in a 7% and 18% higher coupling efficiency than either the 1700μm or 2700μm positions, respectively.

For *imaging arrays*, the extension length resulting in peak directivity should be chosen so as to result in the best possible packing density in the focal plane. For a 13.7mm diameter lens, the aperture efficiency at L_{pk} is 84% at 246GHz and 72% at 500GHz. The corresponding Gaussicity is high at 246GHz with a value of 88% and drops to 78% at 1THz. At L_{pk}, the reflection loss at the lens-air interface contributes an *additional* 0.5dB (11%) reduction in the Gaussian-coupling efficiency (with or without a $\lambda_m/4$ matching-cap layer) compared to the 2200μm position. It is possible to reduce the reflection loss with a higher directivity feed antenna. The L_{pk} position is advantageous because it results in a high-packing density with only a 15-20% drop in Gaussian-coupling efficiency when compared to the 2200μm-2400μm positions. It is also interesting to compare qualitatively the performance at this position to a corrugated horn. At peak directivity position, the extended hemispherical lens at L_{pk} will result in about 20-25% higher packing densities (i.e. aperture efficiencies) and about 25-40% lower Gaussian-coupling efficiencies (including back-side power loss and a $\lambda_m/4$ matching-cap layer) than a corrugated horn designed for the same f/# system. This is not a high penalty to pay for high-packing densities in imaging arrays.

Finally, all our calculations are presented in R/λ and L/λ and therefore present universal design curves for silicon lenses of different diameters at different frequencies. Similar calculations on quartz lenses are available from the NASA-CSTT/University of Michigan and will be published in the October 1993 International Journal of Infrared and Millimeter Waves.

ACKNOWLEDGEMENTS

This work was supported by the NASA/Center for Space Terahertz Technology at the University of Michigan. We are very grateful to Thomas Büttgenbach, Prof. Jonas Zmuidzinas and Prof. David Rutledge, all at the California Institute of Technology, for their immense contributions to this project. We are also grateful to Dr. Andy Harris, Max-Planck Institute for Extra-Terrestrial Physics, Garching bei München, and Dr. Tony Kerr, NRAO, for their detailed review of the manuscript.

APPENDIX

The electric field of a Gaussian-beam is of the form:

$$\mathbf{E}_{\text{Gauss}}(\theta) = \epsilon_{\text{co}}\, e^{-[\theta/\theta_0]^2} e^{\pm j\pi[\theta/\theta_1]^2} \tag{18}$$

where θ is the direction in the far-field from boresight (assuming circular symmetry), and ϵ_{co} is a unit vector representing the polarization of the beam. In the near-field:

$$\mathbf{E}_{\text{Gauss}}(\text{r}) = \epsilon_{\text{co}}\, e^{-[\frac{r}{w(z)}]^2} e^{-jk[\frac{r^2}{2R(z)}]} \tag{19}$$

where r is the radius in a planar field representation (assuming circular symmetry), $w(z)$ is the waist of the Gaussian-beam, $R(z)$ is the radius of curvature, and ϵ_{co} is a unit vector representing the polarization of the beam. The value θ_0 (or $w(z)$) controls the amplitude term and θ_1 (or $R(z)$) controls the phasing term. The coupling efficiency of an antenna to a Gaussian-beam (Gaussicity) is calculated using the formula $\eta = |< \Psi_{Antenna} | \Psi_{Gauss} >|^2$, which written out in the far field is [28]:

$$\eta_{Gaussicity} = \frac{|\iint[\epsilon_{\text{co}} \cdot \mathbf{F}(\theta,\phi)]\, e^{-(\theta/\theta_0)^2} e^{\pm j\pi(\theta/\theta_1)^2} \sin\theta \text{d}\theta\text{d}\phi|^2}{\iint |\mathbf{F}(\theta,\phi)|^2 \sin\theta \text{d}\theta\text{d}\phi \iint e^{-2(\theta/\theta_0)^2} \sin\theta \text{d}\theta\text{d}\phi} \tag{20}$$

and written out in the near-field is:

$$\eta_{Gaussicity} = \frac{|\iint[\epsilon_{\text{co}} \cdot \mathbf{F}(\text{r},\phi)]\, e^{-(\frac{r}{w(z)})^2} e^{-jk(\frac{r^2}{2R(z)})} \text{rdrd}\phi|^2}{\iint |\mathbf{F}(\text{r},\phi)|^2 \text{rdrd}\phi \iint e^{-2(\text{r}/\text{w}(\text{z}))^2} \text{rdrd}\phi} \tag{21}$$

where $\mathbf{F}(\theta,\phi)$ is the electric field in the far-field pattern of the antenna, and $\mathbf{F}(\text{r},\phi)$ is the electric field in the planar representation. The amplitude and phasing terms are varied to optimize the coupling efficiency (Gaussicity). For high coupling efficiency ($> 80\%$), the near-field Gaussian parameters can be found from a Fourier transform of the far-field Gaussian parameters [23].

REFERENCES

[1] D.B. Rutledge, D.P. Neikirk and D.P. Kasilingam, "Integrated circuit antennas," *Infrared and Millimeter-Waves*, vol. 10, K.J. Button, Ed., New York: Academic Press, pp. 1-90, 1983.

[2] G.M. Rebeiz, "Millimeter-wave and terahertz integrated circuit antenna," *Proceedings of the IEEE*, vol. 80, no. 11, pp. 1748-1770, Nov. 1992.

[3] W.Y. Ali-Ahmad, W.L. Bishop, T.W. Crowe, and G.M. Rebeiz, "An 86-106 GHz Quasi-integrated low-noise schottky receiver," to appear in the April 1993 issue of *IEEE Trans. on Microwave Theory Tech.*.

[4] S.S. Gearhart, C.G. Ling, and G.M. Rebeiz, "Integrated millimeter-wave corner-cube antennas," *IEEE Trans. Antennas Propagat.*, vol. AP-39, no. 7, pp. 1000-1006, 1987.

[5] D.F. Filipovic, W.Y. Ali-Ahmad, and G.M. Rebeiz, "Millimeter-wave double-dipole antennas for high-gain integrated reflector illumination," *IEEE Trans. on Microwave Theory Tech.*, vol. MTT-40, no. 5, pp. 962-967, 1992.

[6] D.B. Rutledge and M. Muha, "Imaging antenna arrays," *IEEE Trans. Antennas Propagat.*, vol. AP-30, pp. 535-540, 1982.
[7] M. Born and E. Wolf, *Principles of Optics* . New York: Permagon Press, pp. 252-252, 1959.
[8] E. Hecht, *Optics, 2nd Edition.* Reading, MA: Addison-Wesley, pp. 129-131, 1987.
[9] H. van de Stadt, Th. de Graauw, A. Skalare, R.A. Panhuyzen, R. Zwiggelaar, "Millimeter and submillimeter studies of planar antennas," *First Int. Symp. on Space Terahertz Technology*, Ann Arbor, MI, pp. 235-255, March 1990.
[10] C.J. Adler, C.R. Brewitt-Taylor, M. Dixon, R.D. Hodges, L.D. Irving, and H.D. Rees, "Microwave and millimeter-wave recievers with integral antennas," *IEE Proc.-H*, vol. 138, pp. 253-257, 1991.
[11] A. Skalare, Th. de Graauw, and H. van de Stadt,"A planar dipole array antenna with an elliptical lens," *Microwave and Optical Tech. Lett.*, vol. 4, no. 1, pp. 9-12, 1991.
[12] D.F. Filipovic, S.S. Gearhart, and G.M. Rebeiz, "Double-slot and log-periodic antennas on extended hemispherical dielectric lenses," in *Proc. 3rd Int. Conf. Space Terahertz Technology*, Ann Arbor, MI, pp. 382-393, March 1992.
[13] R.H. Duhamel and D.E. Isbell, "Broadband logarithmically periodic antenna structure," *IRE National Convention Record*, Part I, pp. 119-128, 1957.
[14] J.D. Dyson, "The Unidirectional Equiangular Spiral Antenna," *Trans. IRE*, AP-7, pp. 329-34, 1959.
[15] T.H. Büttgenbach, "A fixed tuned broadband matching structure for submillimeter SIS receivers," to appear in the Sept. 1992 issue of *IEEE Trans. on Applied Superconductivity.*
[16] Q. Hu, Z.A. Mears, P.L. Richards, and S.L. Loyd, "Millimeter-wave quasioptical SIS mixers," *IEEE Trans. Magn.*, vol. 25, pp. 1380-1383, 1989.
[17] J. Zmuidzinas, "Quasi-Optical Slot Antenna SIS Mixers," *IEEE Trans. on Microwave Theory Tech.*, vol. MTT-40, no. 9, pp. 1797-1804, 1991.
[18] A. Skalare, H. van de Stadt, Th. de Graauw, R.A. Panhuyzen, and M.M.T.M. Dierichs, "Double-dipole antenna SIS receivers at 100 and 400 GHz," in *Proc. 3rd Int. Conf. Space Terahertz Technology*, Ann Arbor, MI, pp. 222-233, March 1992.
[19] T.H. Büttgenbach, "An improved solution for integrated array optics in quasi-optical mm and submm receivers: the hybrid antenna," to appear in this issue of *IEEE Trans. on Microwave Theory Tech.*.
[20] A.R. Kerr, P.H. Siegel, and R.J. Mattauch,"A simple quasi-optical mixer for 100-120GHz," *IEEE-MTT Int. Microwave Symp. Digest*, pp. 96-98, 1977.
[21] R.S. Elliott, *Antenna Theory and Design.* New Jersey: Prentice-Hall, Chap. 4, 1981.
[22] M. Kominami, D.M. Pozar, and D.H. Schaubert, "Dipole and slot elements and arrays on semi-infinite substrates," *IEEE Trans. Antennas Propagat.*, vol. AP-33, pp. 600-607, June 1985.
[23] R.E. Collin, *Antennas and Radiowave Propagation.* New York: McGraw-Hill, Chap. 4, 1985.
[24] C. A. Balanis, *Antenna Theory: Analysis and Design.* New York: Wiley, Chap. 11, 1982.
[25] K.C. Gupta, R. Garg, and I.J. Bahl, *Microstrip Lines and Slotlines.* Dedham, Massachusetts: Artech House, Chap. 7, 1979.
[26] R. Johnson and H. Jasik; *Antenna Engineering Handbook, 2nd Edition.* New York: McGraw-Hill, Chap 16, 1984.
[27] A. Yariv and P. Yeh, *Optical Waves in Crystals.* New York: Wiley, Chap. 2, 1984.
[28] S.E. Schwarz, "Efficiency of quasi-optical couplers," *Int. J. Infrared Millimeter Waves*, vol. 5, pp. 1517-1525, 1984.